Biomacromolecules

pubs.acs.org/Biomac

Article

Effect of Surface Modification on the Pulmonary and Systemic Toxicity of Cellulose Nanofibrils

Kukka Aimonen, Mira Hartikainen, Monireh Imani, Satu Suhonen, Gerard Vales, Carlos Moreno, Hanna Saarelainen, Kirsi Siivola, Esa Vanhala, Henrik Wolff, Orlando J. Rojas, Hannu Norppa, and Julia Catalán*

Cite This: *Biomacromolecules* 2022, 23, 2752–2766

Read Online

ACCESS | Metrics & More | Article Recommendations | Supporting Information

ABSTRACT: Cellulose nanofibrils (CNFs) have emerged as sustainable options for a wide range of applications. However, the high aspect ratio and biopersistence of CNFs raise concerns about potential health effects. Here, we evaluated the in vivo pulmonary and systemic toxicity of unmodified (U-CNF), carboxymethylated (C-CNF), and TEMPO (2,2,6,6-tetramethyl-piperidin-1-oxyl)-oxidized (T-CNF) CNFs, fibrillated in the same way and administered to mice by repeated (3×) pharyngeal aspiration (14, 28, and 56 μg/mouse/aspiration). Toxic effects were assessed up to 90 days after the last administration. Some mice were treated with T-CNF samples spiked with lipopolysaccharide (LPS; 0.02–50 ng/mouse/aspiration) to assess the role of endotoxin contamination. The CNFs induced an acute inflammatory reaction that subsided within 90 days, except for T-CNF. At 90 days post-administration, an increased DNA damage was observed in bronchoalveolar lavage and hepatic cells after exposure to T-CNF and C-CNF, respectively. Besides, LPS contamination dose-dependently increased the hepatic genotoxic effects of T-CNF.

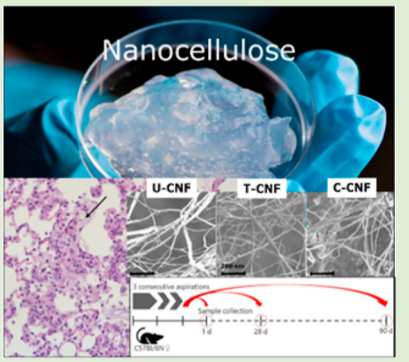

INTRODUCTION

Cellulose nanomaterials have raised great expectations in recent years as sustainable and environmentally friendly alternatives to their mineral or synthetic counterparts.[1] Their unique properties, such as gas barrier properties, high mechanical strength and elastic modulus, shear thinning behavior, and low thermal expansion, allow their use in a large range of applications.[1,2] As such, cellulose nanomaterials are being applied in packaging, composites, emulsions, foams, electronics, cosmetics, medical devices, and tissue engineering scaffolds, among others.[2−4]

Cellulose nanofibrils are obtained from wood and other sources by mechanical deconstruction of cellulose fibers into smaller fibrils through a fibrillation process.[5] Chemical pretreatments are usually applied prior to fibrillation to ease deconstruction into homogeneous fibril dispersions and to confer the nanofibrils with specific properties for different applications.[5,6] TEMPO (2,2,6,6-tetramethyl-piperidin-1-oxyl)-mediated oxidation and carboxymethylation are among the most frequently applied surface modifications to introduce negative charges onto cellulose fiber surfaces.[7,8] It is worth noting, as a no fibrillation process is totally efficient, that the resulting dispersions contain not only fibrils with sizes in the nanoscale but also larger fibrils (microfibrils).[1,9] Moreover, surface modification not only affects the fibrillation yield and surface charge of the fibrils but also other properties like their dimensions, colloidal stability, and specific surface area.[7] TEMPO-mediated oxidation is known to provide homogeneous aqueous dispersions.[10] Furthermore, in addition to cellulose, other wood cell wall components, such as hemicelluloses and lignin, can also be present in small amounts in the dispersions of cellulose fibrils.[1] For the sake of simplicity, herein, we will use the term "cellulose nanofibrils" (CNFs) to generally refer to fibrillated cellulose.

The increasing commercial use of CNFs requires that the safety of these materials for human health and the environment be ensured.[2,11,12] The fibrous nature of CNF, together with the reported high biopersistence,[13−15] raises concerns about the potential health effects that nanofibrils could cause, especially if inhaled.[11] The main route of exposure in occupational settings is via inhalation,[12] where workers may be exposed to airborne CNFs, for example, during drying or spraying processes,[16] or when handling dry materials.[2]

Although an increasing number of studies have addressed the toxicity of cellulose nanomaterials in the last few years,[5,17] reports on potential adverse health effects of CNFs are still sparse. Moreover, the small set of reports available reveals conflicting results for CNF-induced toxic effects, which is partly due to the large range of nanomaterial types and

Received: January 17, 2022
Revised: May 19, 2022
Published: June 9, 2022

https://doi.org/10.1021/acs.biomac.2c00072
Biomacromolecules 2022, 23, 2752−2766

properties arising from the fiber source and the production method, which can modulate toxic response to CNF.[4] For instance, surface chemistry strongly determines how CNF interacts with their environment, governing rheological and interfacial properties and colloidal stability.[4,17] The potential toxicological effects of CNFs that only differ in surface chemistry have thus far been evaluated by a few in vitro studies.[3,18,19] Although in vitro models are appropriate for identifying acute effects and elucidating some primary mechanisms of action, they do not provide information on the behavior of the materials in complex systems, such as whole organisms.[17] In vivo studies, on the other hand, allow the detection of health effects over a longer time span than cell culture-based assays and can reveal secondary mechanisms of action.

To date, the pulmonary effects of CNF have only been investigated in a few in vivo studies.[14,15,20−22] All of them were performed by exposing animals through intratracheal instillation or (oro)pharyngeal aspiration, both of which have been reported to be reliable methods for assessing the pulmonary outcomes of fibrous materials.[21,23] These studies only concerned acute or sub-acute effects (up to 28 days post-exposure) and involved CNFs from different sources or produced by different methods. Therefore, comparisons among different types of CNF have been hampered by the multiple variables affecting the results. A TEMPO-oxidized CNF (300−1000 nm in length and 10−25 nm in width) administered by pharyngeal aspiration (10−200 μg/mouse) induced an acute inflammatory response and increased DNA damage in the lungs of C57Bl/6 mice at 24 h post administration.[20] Four different CNFs manufactured by two different companies—two enzymatically pre-treated CNFs (2−20 μm in length and 2−20 nm in width), one carboxylated CNF (0.5−10 μm in length and 4−10 nm in width), and one carboxymethylated CNF (5−50 μm in length and 3−10 nm in width), together with the bulk-sized material—were assessed for their immunogenic and genotoxic potential using the same animal model and dose range.[14,15] In addition, one of the enzymatically pre-treated CNFs and the carboxylated CNF were also assessed in C57Bl/6 mice intratracheally instilled with 6 and 18 μg/mouse.[22] The enzymatically pre-treated CNFs triggered inflammation more efficiently than those modified by carboxylation or carboxymethylation, although the inflammatory response subsided within a month.[15] Besides, carboxylation reduced the systemic acute phase response.[22] The enzymatically pre-treated CNFs, as well as the bulk fibers, induced more DNA damage in the lung than carboxylated and carboxymethylated CNFs, the damage being still observed 28 days after the administration. The carboxymethylated CNF and both enzymatic CNFs also showed significant DNA damage in bronchoalveolar lavage (BAL) fluid.[14] Increased DNA damage was also observed in the lung tissue and BAL fluid of mice 28 days after intratracheal instillation of the enzymatic and carboxylated CNFs, respectively.[22] Another study performed with BALB/c mice exposed by aspiration to 40 and 80 μg/mouse of an unmodified CNF (142 ± 14 nm in length and 56 ± 14 nm in width) showed differentiation of T-cells toward a Th1-phenotype induced by the material at 14 days post-exposure.[21]

The generally reported inflammogenic response following pulmonary exposure to CNF may have been induced by the endotoxins carried by nanofibrils. Endotoxins [e.g., lipopolysaccharide (LPS)], bacterial components frequently found as contaminants in cellulosic materials,[24] can trigger toxicological effects when administered to animals.[25,26] As CNFs are typically produced in the absence of aseptic conditions, contamination with endotoxins may occur at any step of the manufacturing process.[26] Therefore, CNFs are usually sterilized by autoclaving or adding biocides before testing. However, it is unclear whether these treatments could affect the toxicological properties of CNFs.

In the present study, we evaluated the in vivo pulmonary and systemic toxicity of unmodified cellulose nanofibrils (U-CNFs) and two functionalized CNFs, carboxymethylated (C-CNFs) and TEMPO-oxidized (T-CNFs). The CNFs were obtained from the same source, fibrillated in the same way, and tested as produced without further treatments. CNFs were administered to mice by repeated pharyngeal aspiration, and the inflammatory and genotoxic effects were assessed up to 90 days after the last administration. In parallel, T-CNF samples spiked with increasing amounts of LPS (0.02−50 ng/mouse/aspiration) were included to assess the potential role of endotoxin contamination. Our findings indicate that all CNFs induced an acute inflammatory reaction that mostly subsided within 90 days, even though the CNF was still present in the lungs at that time point. Pulmonary exposure to anionic-modified CNFs was associated with local or systemic genotoxic effects at 90 days post administration. On the other hand, LPS contamination modulated the hepatic response to CNF at the same time point.

EXPERIMENTAL SECTION

Synthesis and Surface Modification of CNFs. As carried out in a previous study,[27] the CNFs were tested as produced, and no further treatments (e.g., sterilization) that may modify their properties[28] were used. As the processing was performed in a non-sterile bench-scale laboratory, special care was taken during the production processes to prevent bacterial contamination. The surface of all the used equipment was extensively cleaned through consecutive washes with deionized water, ethanol (Altia, Helsinki, Finland), sterile purified water, and endotoxin-free water (Thermo Fisher Scientific, UT, USA). Sterile centrifuge tubes (Thermo Fisher Scientific, UT, USA) and sterile and endotoxin-free water were also used to prepare the samples in aqueous media.[27]

CNFs were sourced as commercially low endotoxins containing bleached sulfite birch-dissolving pulp (UPM Kymmene Oyj, Finland), whose lignin content was below 0.5%. The wood fibers were refined using a laboratory-scale PFI refiner (Hamjern Maskin AB, Norway). The refined fibers were then used as such (unmodified) or treated by TEMPO oxidation or carboxymethylation.

We followed the TEMPO oxidation procedure reported earlier.[29,30] Briefly, 2 g (dry weight basis) of the refined fibers were dispersed in distilled water [200 cm^3, 1% (w/v) solid content] and treated with sodium bromide (NaBr) and TEMPO (1.0 and 0.1 mmol·g^{-1}, respectively). The fiber suspension was stirred for 5 min at 700 min^{-1} (rpm) using an Ultra Turrax mixer (IKA, T 25 digital). Subsequently, 10% NaClO solution was added at a dosage level corresponding to 1.2 mmol·g^{-1} (fiber dry weight basis), and 0.5 M NaOH solution was added dropwise to maintain the pH at 10. After 3 h of TEMPO-mediated oxidation, the fibers were thoroughly washed with distilled water to 1.5% (w/v) solid content, followed by microfluidization (six passes, Microfluidics, M-110 P, Massachusetts, USA). The mild oxidation conditions used in our TEMPO treatment were chosen to produce low charge density fibrillated cellulose, thus minimizing the morphological differences compared with the carboxymethylated fibrils. In this way, our comparisons emphasize the effect of modification types. The preparation of the carboxymethylated fibers was performed according to the method detailed by Im et al.[31] In brief, 1 g (dry weight) of the refined fibers were solvent exchanged to

https://doi.org/10.1021/acs.biomac.2c00072
Biomacromolecules 2022, 23, 2752−2766

ethanol (three times washing in 100 mL of ethanol), concentrated by pressure filtration to a solid content of 18 wt %, and then placed in a round-bottom flask. Following this, the fibers were impregnated with 0.96 mmol·g^{-1} of monochloroacetic acid in 200 mL of isopropanol for 30 min at 35 °C. Then, the fibers were added in a solution of 3.68 mmol·g^{-1} of NaOH dissolved in 300 mL at a volume ratio of 1:4 in a mixture containing methanol and isopropanol, respectively. The pre-treated fibers were washed with water and filtered until pH and conductivity reached 7.0 ± 0.5 and ≤20 μS/cm, respectively.

The unmodified and pre-treated fibers were diluted to 1.5% solid content, and nanofibrils were obtained by disintegration through microfluidization after six cycles (Microfluidics, M-110 P, Massachusetts, USA), as previously reported.[29,30] In this way, CNFs of three different types, unmodified (U-CNFs), TEMPO-oxidized (T-CNFs), and carboxymethylated (C-CNFs), were obtained. The resulting aqueous dispersions were concentrated by slow evaporation in an oven until reaching a 1.0−1.5% concentration, which was considered adequate for toxicity testing.

Characterization of the CNFs. Characterization was performed as previously described.[27] Atomic force microscopy (AFM) was used to investigate the morphology of the CNF samples using a Dimension 5000 scanning probe microscope (Veeco, TX, USA). The measurements were performed in tapping mode using a Veeco Nanoscope with a V controller (Veeco) in the air using MicroMash silicon cantilevers (NSC15/AIBS). Samples were prepared by placing the respective CNF aqueous dispersion (0.001 wt %) in an ultrasonic bath (240 W, 50/60 Hz; BANDELIN, Germany) for 30 min. A droplet of the CNF aqueous dispersion was cast onto a microscope glass slide and allowed to dry at room temperature for 24 h.

Scanning electron microscopy (SEM) analyses were carried out using a field emission gun scanning electron microscope (FEG-SEM; Zeiss Sigma VP, Jene, Germany) at an acceleration voltage of 1.5 kV with a field emission gun. For this purpose, the CNF aqueous dispersions were freeze-dried (0.001 wt %) overnight and gold-sputtered to a thickness of 5 nm. The images obtained from the AFM and SEM analyses were subjected to ImageJ (USA) analysis by using 100 nanofibrils from each CNF sample, as recommended by Foster et al.,[4] to yield the respective size distribution profile.

The yield of the production of the nanofibrils was evaluated by centrifuging a 0.2 wt % cellulose fibril suspension (40 mL) at 9000 rpm for 30 min. The percentage of supernatant material provided an estimation of the yield of fibrillation.[32]

The crystallinity of the freeze-dried CNFs was determined by the X-ray diffraction (Model X'Pert Pro, Philips PANalytical, Netherlands) spectra. The samples were scanned in the range of $2\theta = 5-50°$ using a scanning rate of 0.5° min^{-1} at 45 kV voltage and 40 mA electric current.

The electrostatic charge was assessed by using ζ-potential measurements. Dispersions of 0.001% (w/w) of the CNF samples were prepared in water through ultrasonication for 60 s using a universal dip cell in a Zetasizer Nano instrument (Nano ZS, Malvern Instruments Ltd, Worcestershire, UK). Three repeated measurements per sample were conducted at 25 °C.

The concentration of carboxyl groups (COOH) was determined by conductivity titration. Briefly, a dried sample (∼50 mg) was mixed with deionized water (20 mL) and 0.01 M HCl (15 mL), and the mixture was stirred while the pH was set to 3.0 with HCl. Then, a 0.01 M NaOH solution was added until pH 11. The carboxylate content of the samples was determined from the sudden change in conductivity. To determine the aldehyde content (−CHO), a suspension of 10% cellulose/water mixture (20 g) was mixed with deionized water (100 mL) and adjusted to pH 4. An excess amount of 5% w/w hydroxylamine hydrochloride solution was added to the sample, set to pH 4 using 0.05 M NaOH, and allowed to react for 2 h. The aldehyde concentration in the sample was determined through the Schiff base reaction that converts the aldehydes to oximes and is calculated from the moles of NaOH consumed to reach pH 4.[33,34]

The content of bacterial lipopolysaccharides (endotoxin levels) was measured using the Pierce Chromogenic Endotoxin Quant Kit (Thermo Fisher Scientific, Waltham, MA, USA) according to the manufacturer's instructions. This kit has no interference from β-glucans. All samples were heated at 75 °C for 15 min, prior to the endotoxin test, to promote the release of endotoxins from the material as previously described.[26]

CNF Dispersion. Stock dispersions (2 mg mL^{-1}) were prepared in endotoxin-free water by diluting the CNF aqueous dispersions and were then mixed vigorously by high-speed vortexing for 20 s, as recommended by Bitounis et al.[35] Then, serial dilutions were prepared in water and mixed by vortexing for 20 s immediately before being administered to mice.

Animals. Female C57BL/6 mice (7−8 weeks old, average weight of 20 g) were obtained from Scanbur AB (Sollentuna, Sweden) and quarantined for 1 week. The mice were randomly assigned to groups of 3−4 animals/cage and housed in ventilated plastic cages bedded with aspen chip. The animals were kept in a controlled environment with a 12 h dark/light cycle, a temperature of 20−21 °C, and relative humidity of 40−45%. They were provided with a standard rodent chow diet and tap water ad libitum. The weight of the mice was recorded at the beginning and in the end of the experiment, and the health status was carefully monitored throughout the experiment. The experimental procedures agreed with the European Convention for the Protection of Vertebrate Animals Used for Experimental and Other Scientific Purposes (Strasbourg, March 18, 1986, adopted in Finland on May 31, 1990). The study was approved by the Animal Experiment Board and the State Provincial Office of Southern Finland (license number ESAVI/31843/2019).

Pharyngeal Aspiration Exposure. Pharyngeal aspiration exposure was performed as previously described.[36] Three (1 day post-exposure) or six (28 and 90 days post-exposure) mice per group were exposed to repeated (3×) doses (50 μL/mouse) of each CNF at 14, 28, and 56 μg/mouse/aspiration, resulting in accumulative doses of 42, 84, and 168 μg/mouse. This range of doses corresponded to the ones tested in previous studies with nanocellulose materials.[14,20,21,37] In addition, it covered realistic levels of human exposure as, in the case of nanocrystalline cellulose, an accumulative dose of 240 μg/mouse was reported to be equivalent to the dose of a human worker exposed for 42 working days to the U.S. Occupational Safety and Health Administration's (OSHA) 5 mg m^{-3} permissible exposure limit for the respirable fraction of cellulose dust.[38] On the other hand, after assessment of nanocrystalline cellulose facilities, the maximum estimated concentration of detected airborne cellulose was more than 10 times below the OSHA limit.[12] Vehicle control mice received 50 μL/aspiration of endotoxin-free water. A positive control group was included for the inflammatory response and the induction of micronuclei. Within this group, each animal received a pharyngeal aspiration of 28 μg of multiwalled carbon nanotubes (MWCNTs; MWCNT-XNRI-7 from Mitsui & Co., Ltd., Tokyo, Japan), and at 28 and 90 days post-exposure also, a single dose of 40 μg of mitomycin C (MMC, Sigma-Aldrich, Steinheim, Germany) was intraperitoneally injected 48 h before euthanizing the animals. MWCNTs were included due to their capacity to induce acute and sub-acute pulmonary inflammation in mice[15] and were dispersed as previously described.[39] MMC is a genotoxic compound recommended to be used as a positive control in the in vivo micronucleus assay.[40] The mice were euthanized by an overdose of isoflurane at 1, 28, and 90 days after the last exposure.

The potential effects of endotoxin contamination were assessed by including additional groups of mice that were treated with T-CNF samples (14 μg/mouse/aspiration) spiked with increasing amounts of LPS (0.02, 1, and 50 ng/mouse/aspiration). T-CNF was chosen as the carrier of LPS, as this type of functionalization has been reported to render low levels of endotoxin contamination.[41] To ensure an LPS-induced inflammatory response, 50 ng/mouse/aspiration, which has previously been reported to induce a strong acute inflammation in mice,[42] was chosen as the highest dose. This dose corresponded to 10^4 EU mL^{-1} of LPS. The two lower doses (1 and 0.02 ng/mouse/aspiration) corresponded to 200 and 4 EU mL^{-1}.

For all the analyzed endpoints, the unmodified and surface-modified CNF were compared with the vehicle group, whereas the LPS-spiked T-CNF samples were compared with the corresponding

https://doi.org/10.1021/acs.biomac.2c00072
Biomacromolecules 2022, 23, 2752−2766

T-CNF treatment (the uncontaminated T-CNF at 14 μg/mouse/aspiration).

Sample Collection. Blood was collected from the vena cava, mixed with 5% ethylene diaminetetraacetic acid (EDTA; Merck KGaA, Darmstadt, Germany) in a tube (to prevent coagulation), and stored on ice. The trachea was cannulated with a blunted 22-gauge needle, and bronchoalveolar lavage (BAL) was performed once with 800 μL of phosphate buffered saline (PBS; Lonza, Walkersville, MD, USA) to collect a BAL sample for the enumeration of inflammatory cells and transmission electron microscopy (TEM) analyses, and then infused four times with 800 μL of 0.15 M NaCl (Baxter Healthcare SA, Zurich, Switzerland) to collect a BAL sample for the comet analyses. Both BAL samples were stored on ice until being processed. The chest of the mouse was opened, and the right lung lobules were removed and placed into a tube containing cold Merchant's medium for the comet assay. Pieces of the liver were processed in a similar way. The rest of the lung and pieces of the liver were fixed in 10% formalin for histopathological analyses, and a piece of the lung was fixed with 2.5% glutaraldehyde and prepared for TEM analyses.

BAL Fluid Cellularity. One hundred μL of the first BAL sample was cytocentrifuged onto a microscope slide, air dried and stained with May-Grünwald-Giemsa (MGG; Reagena, Toivala, Finland). A minimum of 100 inflammatory cells (classified as macrophages, neutrophils, eosinophils, or lymphocytes) per animal were analyzed using a Zeiss Axioplan light microscope (Carl Zeiss Microscopy GmbH, Göttingen, Germany) at 40× magnification. Another aliquot (100 μL) was used to determine the total number of inflammatory cells using a flow cytometer (CytoFLEX S, Beckman Coulter, Indianapolis, IN, US).

Histological Evaluation. Tissue sections of the lung and liver collected in 10% formalin were fixed for 24 h at room temperature. Then, the samples were embedded in paraffin, cut, affixed on slides, and stained with hematoxylin and eosin as previously described.[39] The slides were examined with a light microscope (Zeiss Axioplan, Carl Zeiss Microscopy GmbH, Göttingen, Germany), and the scoring of different histological events was based on a subjective semi-quantitative assessment, as previously described.[43] The different events included in the analysis were: (i) macrophage infiltrates (which refers to dense collections of >10 cells), (ii) lymphocyte aggregates (which refers to dense collections of >20 cells), (iii) neutrophilic aggregates (which refers to dense collections of >10 cells), (iv) eosinophilia (an infiltration of eosinophils into the lung), (v) free material in the bronchial and alveolar space, and (vi) granuloma (material surrounded by a dense macrophage layer).

Lung Biopersistence. The presence of CNF and MWCNTs in the lung tissue was assessed at all time points by light microscopy in association with the histopathological evaluation. As light microscopy only allows the detection of material aggregates, TEM was used to assess whether nanofibrils were located inside the alveolar or bronchial spaces or within cells at 90-days post-exposure. BAL and lung samples were fixed in 2.5% glutaraldehyde at 4 °C for 24 h and thereafter stored refrigerated in PBS. Then, samples were placed onto uncoated copper grids, post-fixed in osmium tetroxide, and stained with uranyl acetate and lead citrate, as described previously.[44] Samples were analyzed using a Jeol JEM-1400 Flash transmission electron microscope (Jeol Ltd, Tokyo, Japan) operated at an acceleration voltage of 80 kV and equipped with a Matataki Flash sCMOS camera (Jeol Ltd, Tokyo, Japan).

Comet Assay from BAL, Lung, and Liver Suspensions. DNA damage was assessed by the comet assay in mouse samples collected at 28- and 90-day post-exposure and processed as previously described.[39] In brief, pieces of the lung and liver were minced in chilled Merchant's medium and mechanically dispersed into a single-cell suspension using a cell strainer (40 μm Ø; VWR International LLC, Radnor, USA). A small proportion of cell suspensions were exposed to hydrogen peroxide (H_2O_2, 100 μM) ex vivo and used as an internal positive control to verify the performance of the comet assay. The alkaline version of the comet assay (pH > 13) was performed as described previously.[45] One scorer analyzed coded slides using a fluorescence microscope (Axioplan 2, Zeiss, Jena, Germany) and an interactive automated comet counter (Komet 5.5, Kinetic Imaging Ltd., Liverpool, UK). The percentage of DNA in the comet tail was analyzed from two slides per animal (75 cells/slide and 150 cells/animal) to measure the amount of DNA damage.

Micronucleus Assay in Peripheral Blood Erythrocytes. Systemic chromosome damage was assessed by the micronucleus assay in mouse samples collected at 28- and 90-days post-exposure. Blood samples were diluted 1:5 in fetal bovine serum (Life Technologies Limited, Paisley, UK), smeared onto microscopical slides, dried at room temperature overnight, and fixated in methanol (Merck KGaA, Darmstadt, Germany). The slides were stained with MGG, and the micronucleus analysis was performed in accordance with TG 474.[40] Stained slides were analyzed using a light microscope (Zeiss Axioplan, Carl Zeiss Microscopy GmbH, Göttingen, Germany) at 40× magnification. Two thousand normochromatic erythrocytes (NCEs) per animal were scored for the frequency of micronucleated normochromatic erythrocytes (MNCEs). In addition, 2000 polychromatic erythrocytes (PCEs) per animal were scored in the vehicle and the positive control group for the frequency of micronucleated polychromatic erythrocytes (MPCEs). Besides, the ratio of PCEs to NCEs was assessed in 2000 erythrocytes per animal as an indicator of bone marrow toxicity.

Statistical Analyses. Statistical analyses of the body weight, neutrophils, and other cell counts in BAL, cell aggregates/infiltrates in the lungs, the frequency of micronucleus and the percentage of PCEs were performed as described by Hadrup et al.[46] Data were tested for normality with the Shapiro−Wilk test, and for homogeneity of variance with the F test or the Brown−Forsythe test (for two or more than two sample comparisons, respectively). In the case of deviations in normality or in homogeneity of variance, the non-parametric Mann−Whitney (two groups) or Kruskall−Wallis (more than two groups) tests were applied. Otherwise, differences were assessed by a one-way *t*-test or one-way analysis of variance (ANOVA). In addition, Dunn's and Dunnett's multiple comparisons tests (Kruskall−Wallis test and ANOVA, respectively) were used for an a posteriori comparison of each of the doses with the corresponding zero control.

A hierarchic ANOVA was used to evaluate if the percentage of DNA in tail in BAL and lung cells was influenced by the treatments, as recommended by Bright et al.[47] Bonferroni's test was applied as a posteriori comparison among the means.

For all endpoints analyzed, dose-dependent relationships were investigated by linear regression analysis.

Differences were interpreted to be significant if $p < 0.05$. The analyses were performed using the IBM SPSS Statistics for Windows (2013), Version 22.0 program.

RESULTS

Characterization of the CNF Samples. Figure S1 presents FEG-SEM images of the CNF samples at low magnification, showing the main structural and morphological features of the nanofibrils. They included large fibrils and fragments originated from the cell wall of fibers given the limited extent of fibrillation. Also, it is possible that fibril aggregates are formed upon removal of water during the sample preparation. As shown in Table 1, T-CNF reported the highest fibrillation yield (78%), followed by C-CNF (69%) and U-CNF (58%). In addition, our TEMPO oxidation conditions were rather mild, which led to fibrils of similar sizes compared to the carboxymethylated ones. No significant differences in the lateral fibril width were observed even though T-CNF indicated smaller sizes (Table 1 and Figure 1b,e,h), as it is also generally expected for this CNF grade.

The structural morphology and fibril diameter distributions of the CNF samples are shown in Figure 1. Besides, the average width and length of individual fibrils, as well as the aspect ratio, are shown in Table 1. The T-CNF sample showed the lowest lateral dimension and length, with values in the

https://doi.org/10.1021/acs.biomac.2c00072
Biomacromolecules 2022, 23, 2752−2766

Table 1. Physico-Chemical Characteristics and Endotoxin Levels of the Fibrillated Cellulose Samples[a]

material	U-CNF	T-CNF	C-CNF
surface modification	none	TEMPO oxidation	carboxymethylation
fibrillation yield (%)	54	78	69
degree of crystallinity (%)[b]	75	67	71
fibril width (D) (nm)[c]	11.5 ± 0.07	7.7 ± 0.90	8.5 ± 0.04
length (L) (nm)[c]	2011 ± 301	1589 ± 220	1820 ± 119
aspect ratio (L/D)	175	207	214
ζ-potential (mV)	−19 ± 2	−27 ± 3	−30 ± 1
carboxyl group content (mmol·g^{-1})	0.02	0.41	0.35
aldehyde group content (mmol·g^{-1})	0.014	0.070	0.030
endotoxin level (EU mL^{-1})[d]	>1.2[e,f]	0.22	0.15

[a]Fiber diameter and length, and ζ-potential are expressed as mean ± SD. [b]From Aimonen et al.[27] [c]Determined by atomic force microscopy and scanning electron microscopy. [d]Evaluated using the Pierce Chromogenic Endotoxin Quant Kit. [e]Levels above the 0.5 EU mL^{-1} limit value established by the US Food and Drug Agency (FDA) for inhalation studies. [f]Levels above the detection limit of the kit (1.2 EU mL^{-1}).

range of 7.7 ± 0.9 and 1589 ± 220 nm, followed by the C-CNF and U-CNF samples. The aspect ratio of the nanofibrils varied from 175:1 (U-CNF) to 214:1 (C-CNF), although the observed differences between surface-modified nanofibrils were small. All the samples showed a good degree of colloidal dispersion in water, as judged by direct visual observation of vials containing the given aqueous dispersions.

Table 1 also includes the degree of crystallinity, ζ-potential values, and content of functional groups of the CNF samples. The minimum and maximum degree of crystallinity of the CNF samples varied from 67 to 75% (for T-CNF and U-CNF, respectively), indicating that the chemical modification did not considerably alter the crystallinity of the CNFs. It is known that the ζ-potential value tracks with the charge density, for example, dissociated carboxylic groups on the surface of fibrils. As expected, all the CNF samples were anionic according to their ζ-potential. T-CNF had the highest carboxyl group density and a low aldehyde content (0.07 mmol·g^{-1}) comparable to that of C-CNF. Low levels of carboxyl groups were quantified in U-NFC, which presented the lowest ζ-potential values. A good colloidal stability in aqueous media was observed for the suspension of modified fibrils.

Results from the endotoxin analyses are also shown in Table 1. The level of endotoxin contamination was low for both surface-modified CNFs, with values below the 0.5 EU mL^{-1} limit value established by the US Food Drug Agency for inhalation studies.[48] On the other hand, a high endotoxin level, exceeding the detection limit of the kit (>1.2 EU mL^{-1}), was shown by U-CNF.

Clinical Signs and Body Weight. Along the study period, no clinical signs of toxicity were observed.

A decrease in body weight was observed in mice exposed to the highest dose (56 μg/mouse/aspiration) of U-CNF (p < 0.01) and to MWCNTs (p < 0.0001) at 1 day after the last administration (Figure S2). However, the effect was already reversed for both materials at 28 days post-exposure. No reduction in body weight gain was observed in mice exposed to increasing doses of LPS-spiked T-CNF samples in comparison with the corresponding T-CNF treatment (uncontaminated T-CNF 14 μg/mouse/aspiration).

Neutrophil Counts in Bronchoalveolar Lavage Fluid. BAL fluid cell composition was determined on day 1, 28, and 90 after the last administration (Table S1). Figure 2 shows the results on inflammation measured as neutrophil influx. All CNF samples induced an acute inflammatory reaction on day 1, which was not statistically significant in most of the cases due to the small group size (n = 3). A statistically significant increase in neutrophil count was observed at the highest dose of T-CNF and C-CNF and for the positive control. In addition, C-CNF showed a significantly increasing linear dose−response (p = 0.0002, slope = 463.7).

The initially strong neutrophil influx progressively subsided within 90 days, except for T-CNF. At 28 days post-exposure, a significant increase in neutrophils was present for the middle dose of U-CNF (p = 0.0201), the two highest doses of T-CNF (p = 0.0223 and 0.0016, respectively) and the highest dose of C-CNF (p = 0.0012). In addition, a significantly increasing dose−response was observed for the three CNF samples: U-CNF (p = 0.0053, slope = 15.05), T-CNF (p = 0.0027, slope = 31.80), and C-CNF (p = 0.0031, slope = 23.11).

At 90 days post-exposure, the total number of neutrophils was statistically significantly different from the vehicle level (p = 0.0124) for the highest dose of T-CNF (56 μg/mouse/aspiration) and similar to the number of neutrophils induced by the positive control. Furthermore, T-CNF induced a significantly linear dose−response at this time point (p = 0.0004, slope = 28.5). U-CNF also induced a statistically significant increase in dose−response (p = 0.0148, slope = 14.81), although none of the doses differed from the vehicle group.

Statistically significant increases in the BAL eosinophilic population were observed in mice exposed to T-CNF (1 d post-exposure) and to U-CNF and the positive control (28 d post-exposure). An increased eosinophil influx was induced by none of the materials at 90 d post-exposure (Table S1).

The LPS-spiked samples showed a similar behavior to that of the corresponding uncontaminated T-CNF at 14 μg/mouse/aspiration (Figure 2). After the strong neutrophil influx at 1-day post-exposure, the number of neutrophils dropped at 28- and 90-days post-exposure. No significant linear regression was observed at any of the time points. No significantly increased eosinophil influx was observed at any time point (Table S1).

Histopathology Evaluation. Recorded histopathological changes are presented in Tables S2−S4. In addition, representative images of the most predominant histological changes at each studied timepoint are presented in Figure 3. Vehicle-exposed mice initially showed some inflammatory changes that were resolved at 28- and 90-days post-exposure (Figure 3A). Overall, the differences among the CNF-treated mice samples were minor. At 1-d post-exposure, all CNF materials induced an acute peri-bronchial neutrophilic inflammatory reaction accompanied by eosinophilia (Table S2), as illustrated in Figure 3B. As eosinophilia was recorded as the incidence of animals showing this effect, the results do not allow quantification of the reaction. In addition, macrophage infiltrates were seen in the alveolar region around material aggregates. The initial reaction had mostly resolved at 28 days post-exposure (Table S3 and Figure 3C), but mild dose-dependent peri-bronchial neutrophilic reaction and some

https://doi.org/10.1021/acs.biomac.2c00072
Biomacromolecules 2022, 23, 2752−2766

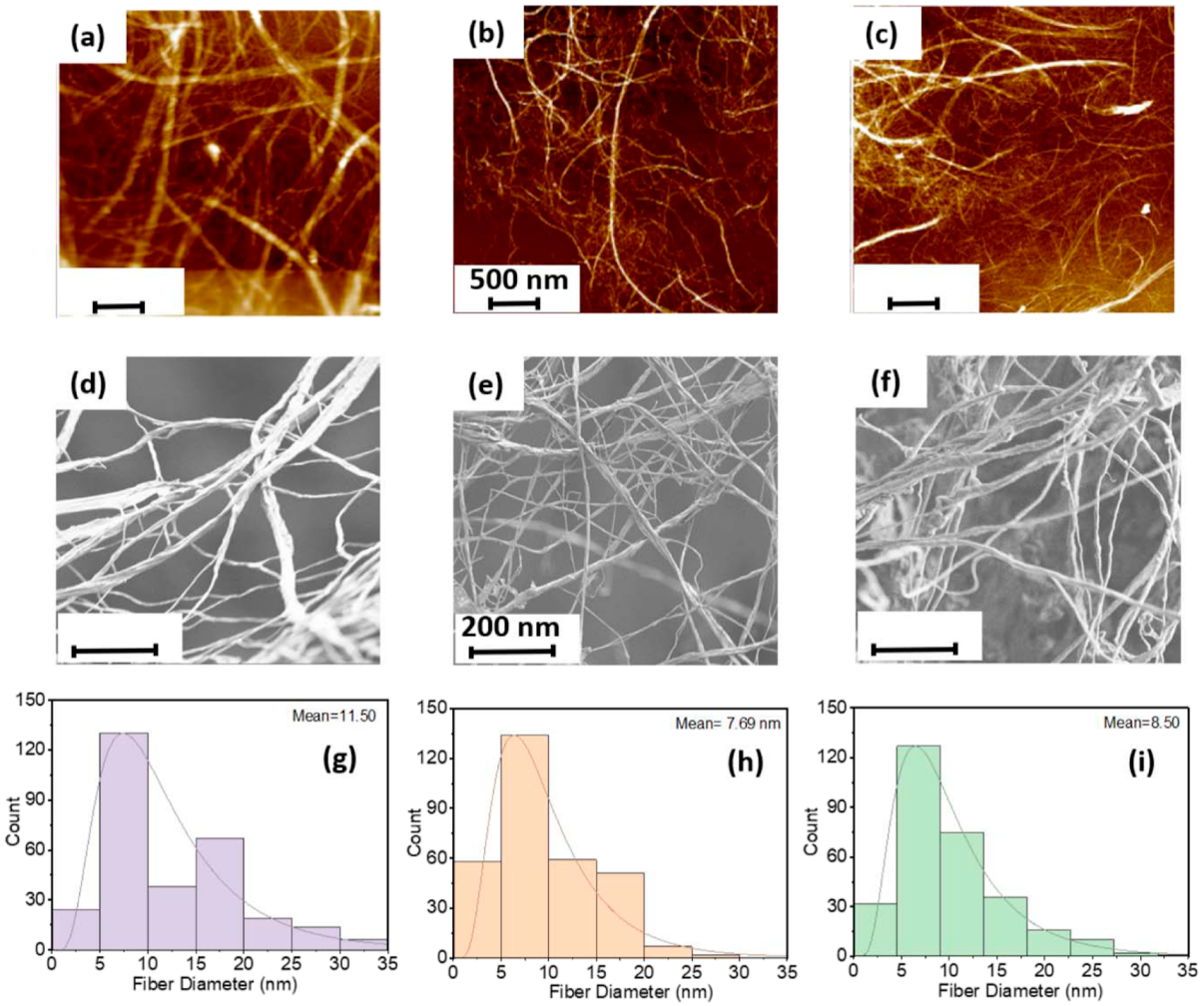

Figure 1. Atomic force microscopy (AFM; top row) and scanning electron microscopy (SEM; middle row) images, and fibril lateral size distributions (fitted log−normal models; bottom row) of U-CNF (a,d,g), T-CNF (b,e,h), and C-CNF (c,f,i).

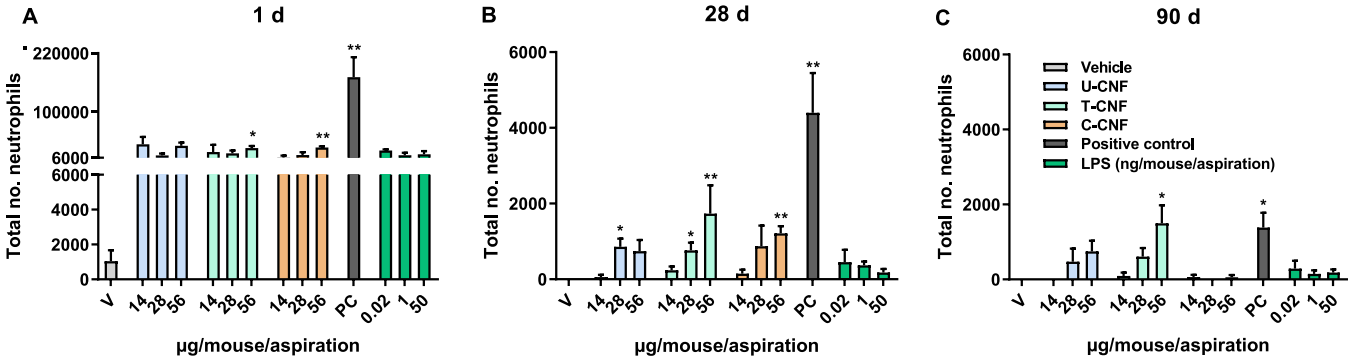

Figure 2. Total number of neutrophils in BAL fluid at 1 (A), 28 (B), and 90 (C) days of the vehicle, CNF samples, positive control, and LPS-spiked T-CNF sample exposure. Data are expressed as mean ± SEM. Asterisks designate statistically significant differences compared with the vehicle group at $*p < 0.05$ and $**p < 0.01$. The LPS-spiked T-CNF samples were compared with the corresponding T-CNF treatment (14 µg/mouse/aspiration), and no significant differences were found.

macrophage infiltrates persisted even at 90 days post-exposure (Table S4 and Figure 3E). Eosinophilic crystals were observed in animals exposed to any type of CNF at 90 days post-exposure (Figure 3D), although no clear incidence of eosinophilia was recorded at this timepoint (Table S4).

The LPS-spiked T-CNF samples induced a slightly stronger neutrophilic inflammatory reaction than the corresponding uncontaminated material (T-CNF, 14 µg/mouse/aspiration) 1-day post-exposure (Table S2), but histopathological changes at 28- and 90-days post-exposure were comparable to the uncontaminated T-CNF sample (Tables S3 and S4).

CNF induced a weaker pulmonary inflammation than the positive control treatment, which included long, straight MWCNTs (28 µg/mouse/aspiration). The positive control

https://doi.org/10.1021/acs.biomac.2c00072
Biomacromolecules 2022, 23, 2752−2766

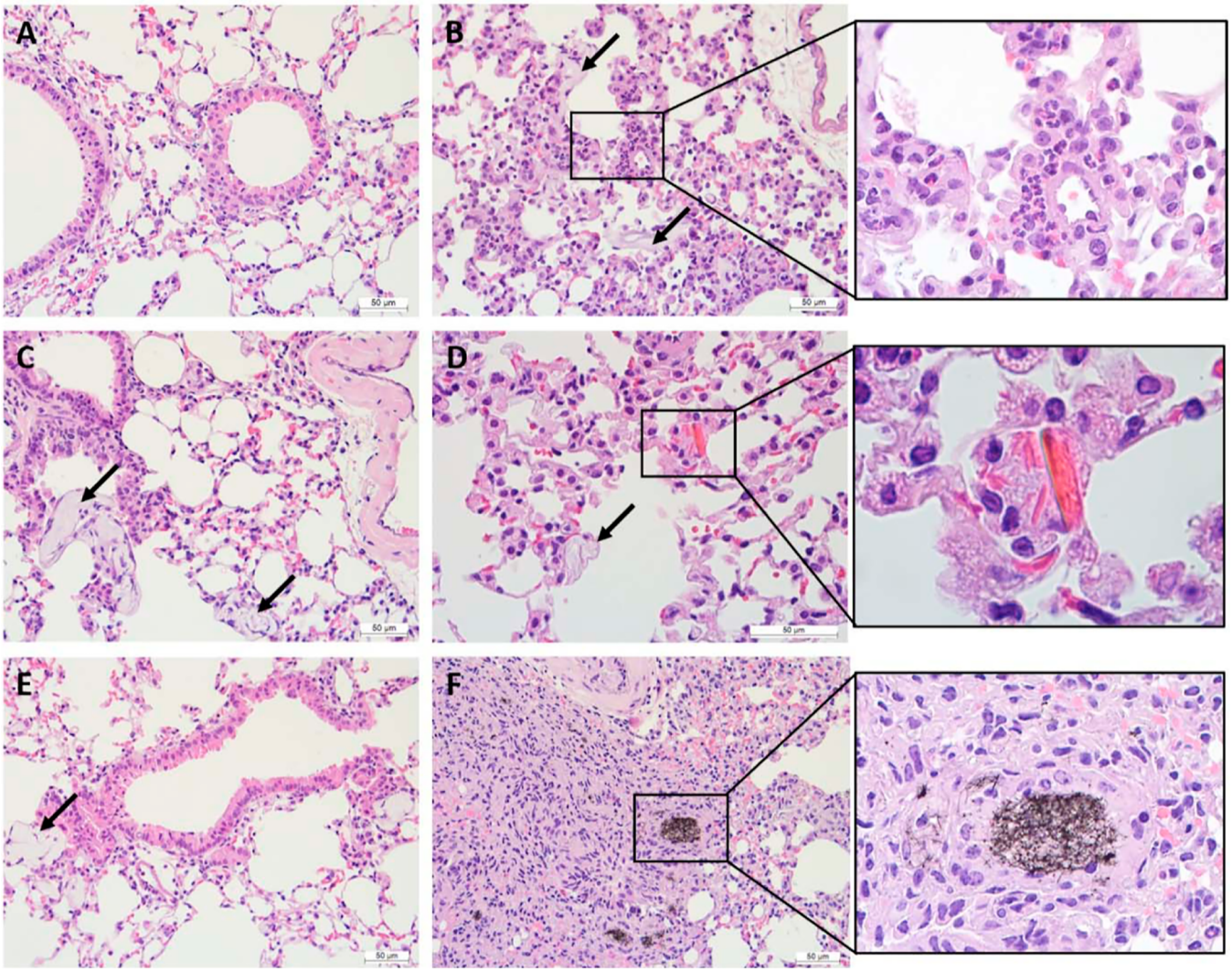

Figure 3. Representative images of hematoxylin- and eosin-stained lung sections of mice exposed to the vehicle (A), CNF [(B−E) 28 μg/mouse/aspiration] or the positive control (F). CNF aggregates are marked with black arrows. (A) Vehicle sample on day 90. (B and inset) Neutrophil influx accompanied by eosinophils in a T-CNF sample 1-day post-exposure. (C) Material in lung tissue in a T-CNF sample 28 days post-exposure. (D and inset) Eosinophilic crystals in a C-CNF sample 90 days post-exposure. (E) Material in lung tissue in a U-CNF sample 90 days post-exposure. (F and inset) Granuloma formation around material aggregates in a positive control sample 90 days post-exposure.

produced a strong acute peri-bronchial neutrophilic reaction and a higher number of macrophage infiltrates in the parenchyma than any of the CNF materials (Table S2). The inflammatory reaction persisted for 28 days after the administration (Table S3). In addition, positive control mice, but not CNF-treated ones, showed signs of granuloma formation in the lung tissue at 90 days post-exposure (Table S4 and Figure 3F).

No histopathological changes were observed in the liver tissue samples for any of the different treatments (data not shown).

Lung Biopersistence. CNF material aggregates were clearly visible both free in the alveolar and bronchial spaces and inside alveolar macrophages at all studied time points (Figure 3B−E). The incidence of animals showing CNF and MWCNT materials in the bronchial and alveolar space remained similar up to 90 days post-exposure (Tables S2−S4). The presence of CNF in the lung tissue at 90-d post-exposure was further confirmed by TEM analyses (Figure 4). A material similar to that identified as CNF was also present in the lung tissue at 24-h post-exposure, but not in samples from the vehicle group at 90-d post-exposure (data not shown).

The previously reported eosinophilic crystals were also observed inside macrophages of the BAL fluid (Figure 4C).

Genotoxicity. Results on the induction of DNA damage, assessed by the comet assay, in the BAL, lung, and liver tissue by different CNF samples at 28-d and 90-d post-exposure are shown in Figure 5. Twenty-eight days after the exposure, only the lowest dose of U-CNF (14 μg/mouse/aspiration) induced a statistically significant increase ($p = 0.031$) in DNA damage in lung cells. At 90-d post-exposure, a significant increase in DNA damage was seen in BAL cells for all three doses of T-CNF tested ($p < 0.001$) with a significant linear dose−response ($p = 0.006$, slope = 0.030). On the other hand, the low, medium, and high doses of C-CNF induced a significant increase in DNA damage in liver cells ($p < 0.05$), with a statistically significant linear dose−response ($p = 0.0348$, slope = 0.023).

The induction of DNA damage by the LPS-spiked T-CNF samples was compared with that of the respective uncon-

https://doi.org/10.1021/acs.biomac.2c00072
Biomacromolecules 2022, 23, 2752−2766

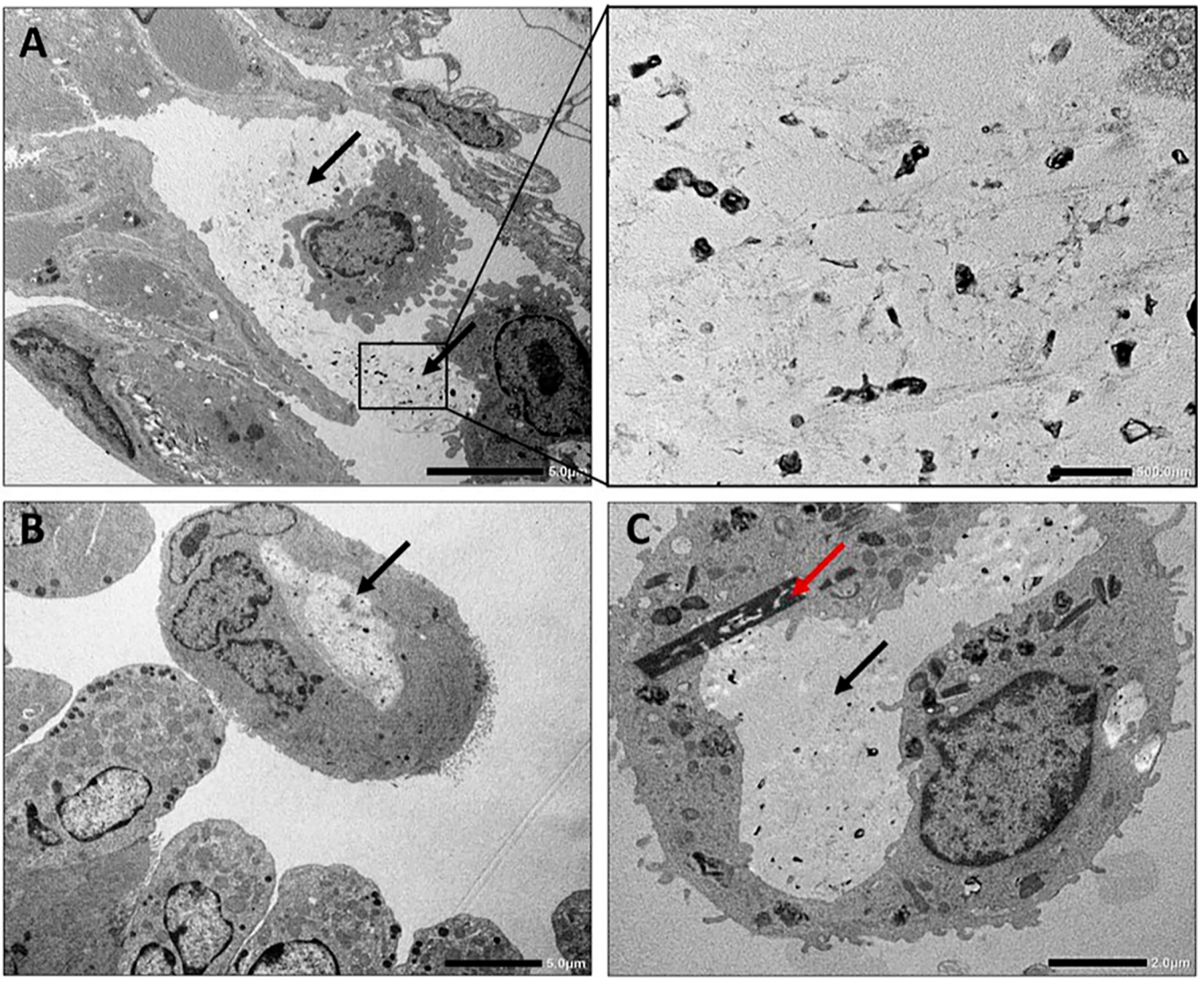

Figure 4. Transmission electron microscope (TEM) micrographs of mouse lung tissue 90 days after repeated pharyngeal aspiration with 14 μg/mouse/aspiration of U-CNF (A,C) or C-CNF (B). Presence of free CNF (black arrows) in the lung parenchyma (A and inset). Bronchoalveolar macrophage containing CNF (B,C, black arrows) and eosinophil crystals (C, red arrow).

taminated sample (T-CNF at 14 μg/mouse/aspiration) in each tissue at both time points (Figure 6). At 28 days after exposure, only the lowest LPS dose (0.02 ng/mouse/aspiration) induced a significant increase ($p = 0.028$) in DNA damage in BAL cells. At 90-d post-exposure, a significant increase in DNA damage was induced in liver cells by all three doses of LPS ($p < 0.05$), and the effect showed a significant linear dose−response ($p = 0.034$, slope = 0.017).

None of the tested CNF samples significantly increased the frequency of micronucleated normochromatic erythrocytes (MNCEs) in peripheral blood at any of the post-administration times (Table S5). The frequency of MNCEs reflects chromosome damage accumulated from the beginning of the treatment until about 60 h before the blood sampling. In all treated groups, the percentage of polychromatic erythrocytes (PCEs) among blood erythrocytes was similar to the values of the vehicle groups, indicating that the CNFs did not show bone marrow toxicity. The positive control treatment (MWCNTs and MMC) significantly increased the frequency of micronucleated PCEs by 12.7-fold in the 28-day series ($p < 0.01$) and 11.6-fold in the 90-day series ($p < 0.01$) in comparison with the vehicle groups. Due to the short exposure time (48 h before the blood sampling), the effect of MMC in the micronucleus assay was analyzed from PCEs—which assesses chromosome damage that occurred 36−48 h before the sampling—and the findings confirmed the validity of the MMC treatment. MMC significantly reduced the percentage of PCEs in the 28-day and 90-day series ($p < 0.01$ and $p < 0.0001$, respectively).

None of the LPS doses induced a significant increase in the frequency of MNCEs in peripheral blood at any of the post-administration times when compared with the corresponding uncontaminated sample (T-CNF at 14 μg/mouse/aspiration) (Table S5). For all LPS treatments, the percentage of PCEs among blood erythrocytes was similar as in the corresponding uncontaminated sample-treated groups, indicating that the contamination with LPS did not induce bone marrow toxicity.

DISCUSSION

In this study, the pulmonary and systemic toxicity of three different types of CNFs (unmodified, carboxymethylated, and TEMPO-oxidized CNFs), produced from the same source of

https://doi.org/10.1021/acs.biomac.2c00072
Biomacromolecules 2022, 23, 2752−2766

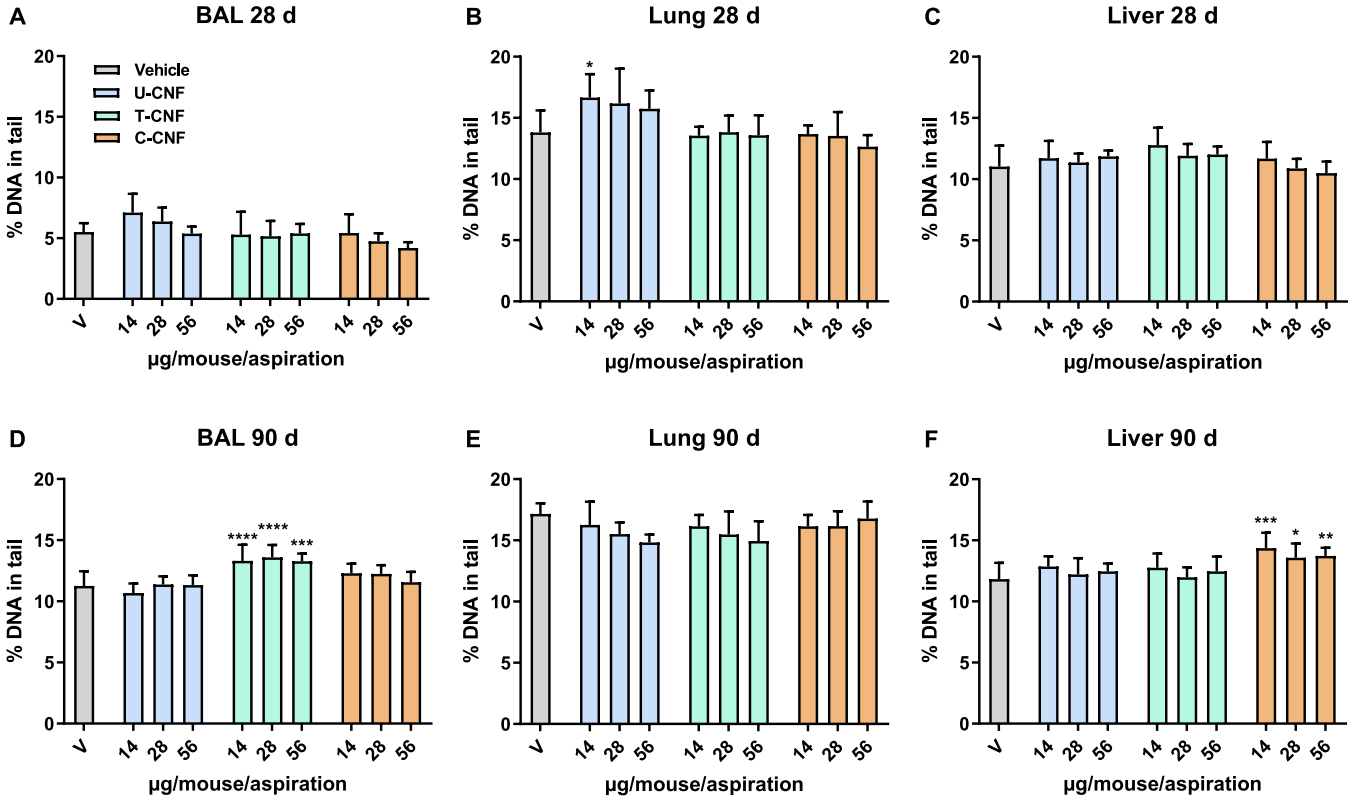

Figure 5. DNA damage (percentage of DNA in the comet tail; mean ± SEM) in the bronchoalveolar lavage (BAL), lung, and liver cells of mice at 28 and 90 days after repeated (3×) pharyngeal aspiration with the vehicle and the CNF samples. Asterisks designate statistically significant differences compared with the vehicle group at $*p < 0.05$, $**p < 0.01$, $***p < 0.001$, and $****p < 0.0001$. A statistically significant increase in the percentage of DNA in the tail over the negative control values was induced by the positive control (H_2O_2, 20 mM) in all the experiments performed (1.94 ± 0.4-fold increase; $p < 0.001$), confirming the validity of the assay (data not shown).

birch pulp fibers and processed in the same way, except for the surface modification steps, were assessed in repeated pharyngeal aspiration-exposed mice for up to 90 days after the last administration. In addition, we investigated the potential role of endotoxin contamination of the fibrils in the observed toxic effects.

The wide applicability of fibrillated cellulose is endowed by introduced surface modifications. Material characterization indicated that the surface charges had a limited influence on the morphology of the fibers, given the mild condition of oxidation used. The fibrils were polydisperse in size (length and width). Fibril fragments were observed for all CNF types, as fibrillation is never fully efficient. The fibrillation yield ranged from 54% (U-CNF) to 78% (T-CNF), which indicates that the proportion of nanofibrils varied among the surface-modified samples. Meanwhile, colloidal stability was observed in agreement with the anionic nature of the samples (ζ-potential between −19 and −30 mV), which promotes electrostatic stabilization,[8] as also reported in other studies.[3,18,19] The results also showed that the nanofibrils produced by TEMPO-mediated oxidation, which is usually an effective method in individualizing CNFs,[10] displayed a relatively smaller lateral dimension (width) compared to other nanofibril types. However, the differences in size between the surface-modified nanofibrils were not significant, and the effects to be discussed below mainly relate to the proportion of micro- and nano-fibrils and the type of surface chemical groups on them.

No remarkable alterations in apparent crystallinity were observed for the fibrillated celluloses with different chemical modifications. A slight decrease in the degree of crystallinity of T-CNF was observed, which can partially be explained by the effect of the oxidation process.[49] Crystallinity may scale with the stiffness of the fibrils, which is considered a key property of fibers' pathogenicity.[50] In fact, stiffness has been identified as one of the determinant attributes of some carbon nanotubes in mesothelioma induction.[51] However, fibrillated cellulose is quite flexible as compared with carbon nanotubes and cellulose nanocrystals and therefore may be more easily engulfed by macrophages and cleared from the body.[52]

Unfortunately, most of the studies assessing the toxicity of fibrillated cellulose do not provide detailed characterization, especially regarding the fibrillation yield and the functional group density. Hence, the results cannot be easily compared. We approach our study based on the type of surface modification, acknowledging that fibrillated celluloses, even if produced using the same modification, do not necessarily track with each other given the differences in charges and other characteristics (surface group density, fibrillation efficiency, etc.). This indeed highlights the complexity of cellulose nano- and micro-fibrils and the need for better standardization.

In the present study, a recruitment of inflammatory cells to the lungs was triggered by the exposure to CNFs. Mice exposed to CNFs and to MWCNTs (and MMC; positive control) displayed an increased influx of neutrophils into BAL one day after the last administration, indicating an acute inflammatory response. Moreover, CNFs—mainly U-CNF and T-CNF—triggered the recruitment of eosinophils into the airways. Supporting the finding in BAL, neutrophils and some

https://doi.org/10.1021/acs.biomac.2c00072
Biomacromolecules 2022, 23, 2752−2766

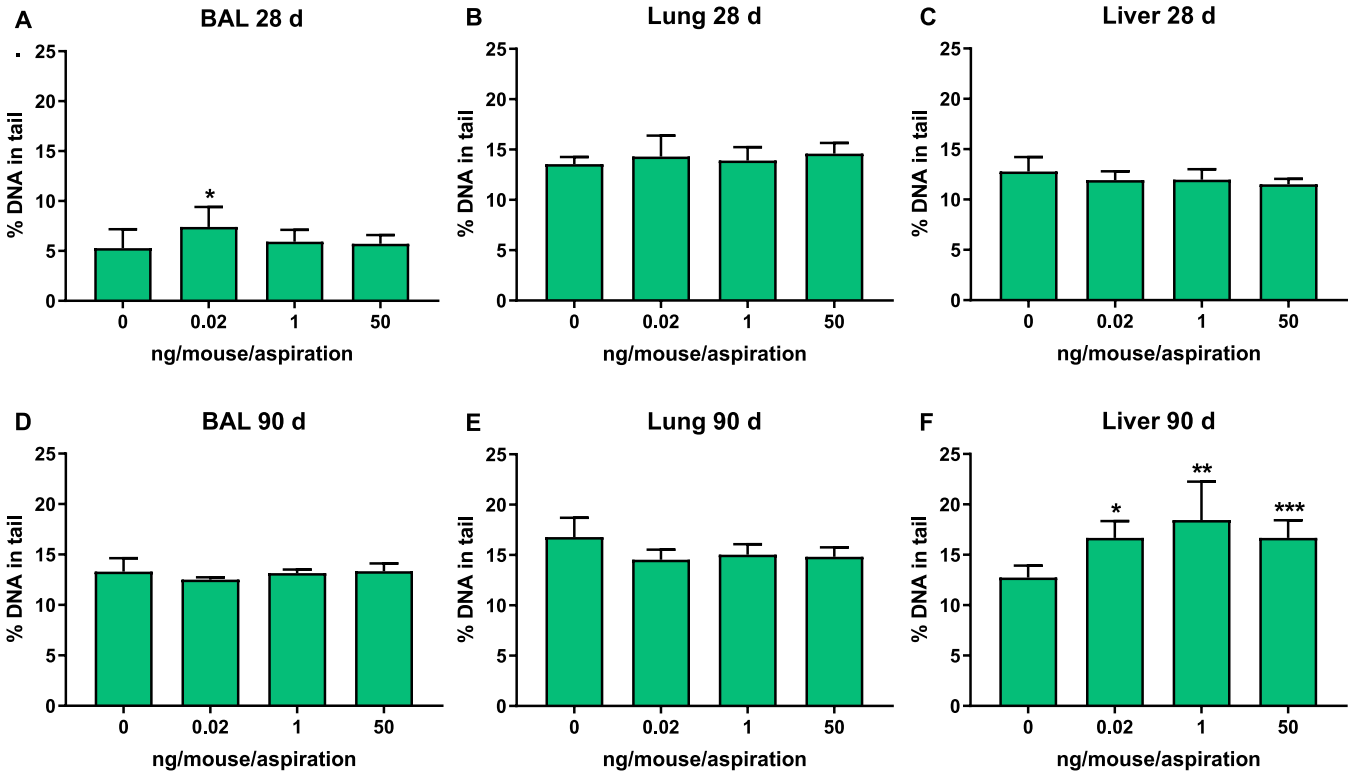

Figure 6. DNA damage (percentage of DNA in comet tail; mean ± SEM) in the bronchoalveolar lavage (BAL), lung, and liver cells of mice 28 and 90 days after repeated (3×) pharyngeal aspiration with T-CNF (14 μg/mouse/aspiration) spiked with 0, 0.02, 1, and 50 ng/mouse/aspiration of lipopolysaccharide (LPS). Asterisks designate statistically significant differences compared with the non-spiked sample at $^{*}p < 0.05$, $^{**}p < 0.01$, and $^{***}p < 0.001$. A statistically significant increase in the percentage of DNA in tail over the negative control values was induced by the positive control (H_2O_2, 20 mM) in all the experiments performed (1.94 ± 0.4-fold increase; $p < 0.001$), confirming the validity of the assay (data not shown).

eosinophils were detected in the lung tissue after all treatments, although the small sample size precluded finding statistically significant differences with the vehicle-treated group. We previously observed similar results with a T-CNF sample (carboxyl content of 1.07 mmol·g^{-1}) administered at similar doses as in the present study, which induced a neutrophilic influx in the small and large bronchia of mice 24-h after a single aspiration.[20]

After 28 days, the initial CNF-triggered acute pulmonary reaction had notably attenuated, although a statistically significant influx of neutrophils into BAL was still observed for all CNFs as well as for the positive control. However, a significant recruitment of eosinophils into BAL was only detected with the middle dose of U-CNF and with MWCNTs. U-CNF also showed a significant number of neutrophilic aggregates and the highest prevalence of eosinophilia in the lung tissue. A similar behavior was previously described for inhaled bulk-sized cellulose fibers, which caused an initially high inflammatory response that subsided after a 28-day recovery period.[53] Our results also conform with those observed by Ilves et al.[15] and Hadrup et al.,[22] who described a more modest immune reaction induced by CNFs at 28 days post-exposure as compared with the acute response observed after 24 h. However, contrary to these studies, carboxylation of CNF (caused by TEMPO oxidation) did not result in a lower inflammation in terms of neutrophilic influx in BAL as compared with the unmodified CNF in the present study.

To the best of our knowledge, no previous studies have assessed the pulmonary effects of CNF after 90 days post-exposure. Among the CNFs, only the highest dose of T-CNF induced a statistically significant influx of neutrophils into BAL at this time point. Interestingly, the total number of neutrophils was similar to that observed at 28 days post-exposure. On the other hand, the neutrophilic influx induced by the positive control dramatically dropped down from 28 to 90 days after exposure. Assuming that MWCNTs contained in the positive control were responsible for the pulmonary effects, at 90 days post-exposure, the total number of neutrophils induced by 28 μg/mouse/aspiration of MWCNTs was similar to that induced by the highest dose of T-CNF (56 μg/mouse/aspiration) and significantly different from the values of the vehicle group. Although neither recruitment of eosinophils into BAL nor incidence of eosinophilia in the mouse lungs were detected with any of the materials at this timepoint, macrophages containing eosinophil-derived crystals were observed with all CNF treatments. The presence of eosinophilic crystals without an inflammatory reaction was earlier reported by Ilves et al.[15] at 28-d post-exposure of CNF. The crystals, which are similar to Charcot-Leyden crystals associated with chronic allergic asthma, are likely formed from the breakdown of earlier recruited eosinophils.[44] The presence of eosinophils and eosinophil crystals suggests that CNF is able to induce a T-helper (Th) 2 type of inflammatory response, earlier seen in association with asbestos and high aspect ratio nanomaterials, but not with granular nanomaterials.[44,54,55] Conversely, a Th1-like immune response was described in BALB/c mice exposed to CNF, whereas a Th2-type immunity was observed after exposing the animals to asbestos.[21]

https://doi.org/10.1021/acs.biomac.2c00072
Biomacromolecules 2022, 23, 2752−2766

The presence of endotoxins in CNF has been suggested as a possible reason for the inflammatory response observed in mice.[14,15] However, endotoxin contamination did not seem to be the reason for the inflammatory effects observed in the present study, as the inflammatory potential of the LPS-spiked T-CNF samples did not differ from the corresponding uncontaminated T-CNF sample, and no LPS dose dependency was seen. The tested LPS dose range (0.02−50 ng/mouse/aspiration) corresponds to $4-10^4$ EU mL^{-1}, which clearly exceeds the reported levels of nanomaterial contamination.[26]

In the present study, CNF-induced local genotoxic effects were assessed by measuring DNA damage in BAL and lung cells. In addition, systemic genotoxicity was assessed by measuring DNA damage in liver cells and the induction of micronuclei in peripheral blood erythrocytes. At 28 days after the exposure, we only detected a significant increase in DNA damage for the lowest dose of U-CNF (14 μg/mouse/aspiration) in lung cells without a significant linear dose−response. In addition, the lowest dose of the LPS-spiked T-CNF sample (0.02 ng LPS/mouse/aspiration) increased DNA damage in BAL cells without a linear dose−response. At 90 days after the exposure, a significant increase in DNA damage was induced by all doses of T-CNF and C-CNF in BAL and liver cells, respectively. A significant increase in linear dose−response was observed with both materials. In addition, the three doses of LPS-spiked T-CNF induced DNA damage in liver cells, showing a significant positive dose−response. Interestingly, neither T-CNF nor C-CNF induced DNA damage at 28 days post-exposure. As the comet assay depicts the level of DNA damage at the time of sampling without showing cumulative effects, the rate of DNA damage or the ratio of DNA damage and DNA repair is higher after 3 months than 1 month for T-CNF in BAL cells and for C-CNF in the liver. Although we do not have information on time points between 28 and 90 days or later, this may indicate that the longer these CNFs stay in the body, the higher the level of continuous DNA damage will be.

Carboxylation and carboxymethylation of CNF have been associated with lower pulmonary DNA damage in mice intratracheally or oropharyngeally treated with modified CNFs compared with mice treated with enzymatically pre-treated CNFs.[14,22] However, none of the materials that were evaluated in vivo induced genetic damage in human bronchial epithelial BEAS-2B cells, suggesting that the mechanisms involved in the genotoxic effects detected in vivo were not present in the in vitro model.[14] Similarly, none of the CNF samples evaluated by Aimonen et al.[19]—including a non-modified enzymatically pre-treated CNF, as well as one CNF sample of the same surface chemistry as C-CNF—increased the frequency of DNA damage or micronuclei in the same cell model. Conversely, the same authors have recently reported a significant induction of micronuclei after treating BEAS-2B cells with the coarse fraction of a carboxymethylated fibrillated cellulose produced in the same way as in the present study.[27] However, neither the medium and fine fractions of the carboxymethylated CNF, nor any of the size fractions of an unmodified and a TEMPO-oxidized CNF, also produced in a similar way as the ones evaluated in this study, induced any genotoxic effect. These findings suggest that the surface chemistry and the size of the fibrils may modulate the capacity of CNF to induce genotoxic effects by primary mechanisms. Primary genotoxicity is due to an interaction of the material with the target cells either by directly damaging the DNA molecule or related proteins, or indirectly by interacting with other cellular organelles (e.g., generating oxidative stress).[56] However, genotoxicity may also rise by secondary mechanisms mediated by inflammation or other intermediate responses not present in the in vitro models. The in vivo genotoxicity may also be due to processes that require longer-term assessment than in vitro assays allow. For instance, depletion of the antioxidant defenses or DNA repair systems. In fact, Ventura et al.[32] reported that a TEMPO-oxidized CNF increased the frequency of micronuclei in adenocarcinomic human alveolar epithelial A549 cells co-cultured with acute monocytic leukemia THP-1 macrophages, a cellular system that has been reported to allow the detection of some mechanisms of secondary genotoxicity.[56] Nonetheless, as both cell types in this co-culture model were simultaneously treated with CNF, the involvement of primary genotoxic mechanisms could not be ruled out. On the other hand, our finding that T-CNF was the only cellulosic material that still induced an inflammatory response in BAL cells after 90 days supports the idea of a secondary induction of DNA damage—mediated by inflammation—for this material.

The fact that both C-CNF and LPS-spiked T-CNF were able to induce DNA damage in the liver 90 days after exposure may indicate that liver cells might be more sensitive than lung cells to either primary or secondary mechanisms of genotoxicity. To show primary genotoxicity, CNF should first be translocated to the liver. Identification of CNF in biological samples is technically challenging.[4,35] CNF would need to be tagged with, for example, fluorescent tags[57] that can affect its surface properties.[58] Hence, we could not detect the materials in the liver. However, other fibrous nanomaterials, for example, MWCNTs, have been reported to be translocated to the liver and induce DNA damage that could still be detected one year after a single intratracheal instillation.[59]

Hepatic genotoxic effects could be caused by the ability of the translocated materials to induce oxidative stress,[60] which has been identified as the main deleterious effect of nanomaterials.[61,62] Alternatively, the genotoxic effects observed in the liver could be caused by circulating inflammatory mediators that are released during pulmonary inflammation.[60] The former hypothesis would be supported by the fact that we observed hepatic DNA damage only at the longest time point, which may reflect the time needed for the materials to translocate in sufficient amounts from the lungs to the liver.[60] In fact, neither the carboxylated nor the enzymatically pre-treated CNFs evaluated by Hadrup et al.[22] induced hepatic DNA damage 28 days after intratracheal instillation, and the authors assumed that this was because the materials had not reached the liver. On the other hand, the carboxymethylated CNF assessed by Aimonen et al.[27] showed the most effective induction of reactive oxygen species (ROS) in BEAS-2B cells, compared with other surface-modified CNFs, in their respective size fractions. Another carboxymethylated CNF (same surface chemistry as C-CNF) was also able to induce the formation of ROS in a dose-dependent manner in BEAS-2B cells[19] but not in THP-1 macrophages.[3] Similarly, two different CNFs neither induced ROS generation nor cytotoxic effects in Kupffer cells,[57] where particles deposited in the liver are primary accumulated.[63] However, no surface modification was reported for any of these CNFs. Furthermore, LPS could have triggered the formation of ROS in liver cells if it were carried by translocated T-CNF, although T-CNF itself would not have induced ROS formation. In fact, endotoxins activate

https://doi.org/10.1021/acs.biomac.2c00072
Biomacromolecules 2022, 23, 2752−2766

Kupffer cells triggering a cascade of biochemical signals in these cells that result in cytokine and ROS production.[64] Regarding the second hypothesis, the original pulmonary inflammation triggered by LPS-spiked T-CNF samples was no longer relevant after 1 month, whereas C-CNF-induced pulmonary inflammation showed similar values to those of the vehicle group. Hence, an inflammation-mediated mechanism does not seem to be involved in these cases.

It is worth noticing that T-CNF and C-CNF did not show big differences in the proportion of nanofibrils (measured by the fibrillation yield), nanofibrils' lateral size, the surface charge, and the functional group densities. However, these small differences, or differences in other parameters related to the surface modification process, seem to influence the biological behavior of the materials. Nevertheless, whatever the mechanisms of action involved, the observed increases in DNA damage were not pronounced, although the effects were dose-dependent in all the cases. The fact that these effects were only detected at the latest time point may also reflect a depletion of the defense mechanisms (e.g., anti-oxidant mechanisms or DNA repair systems) with time as a consequence of continuous DNA damage. If DNA damage persists, it may lead in the long term to carcinogenicity.

All the CNF samples, as well as MWCNTs, showed high biopersistence in the lung tissue. This is in agreement with previous studies of cellulose-based materials.[53] No clearance or degradation of the CNFs present in the mouse lungs was reported to occur within 1 month after exposure.[15] Although CNFs were not quantified in the present study, we observed a similar incidence of animals showing the CNFs in bronchioles and alveolar spaces within the 90-d period. C-CNF had the lowest incidence, in agreement with the previously reported lower number of agglomerates and the smaller total area of agglomerates of this CNF in the lung compared with the other CNF types studied by Ilves et al.[15] As the initial administered dose was the same for all the materials, these findings could reflect a lower agglomeration status of C-CNF, with individualized nanofibrils being more difficult to be detected. However, opposite to MWCNTs—which also showed high biopersistence—no granuloma formation was observed in any of the CNF-treated mice. Similar results were previously reported for the CNFs analyzed by Ilves et al.[15] Therefore, although CNF showed some features of a Th2 type of inflammatory response that is also associated with other high aspect ratio nanomaterials, our findings support the hypothesis that the toxic pulmonary response induced by CNF may differ from that caused by carbon nanotubes or asbestos.[12,21] The difference may partly be due to the higher flexibility of CNF, which will not result in frustrated phagocytosis unlike stiff fibers (e.g., asbestos).[21]

CONCLUSIONS

In summary, the findings presented here suggest that different parameters related to the surface modification of CNF (surface functional group density, fibrillation yield, ...) can affect the evolution of the acute inflammatory response and the generation of DNA damage induced by the material when administered to the lungs. Furthermore, CNF might be translocated from the lungs to the liver, causing DNA damage. The high biopersistence of CNF, together with the reported genotoxic effects, raises concerns about potential carcinogenicity in a long-term pulmonary exposure. The carcinogenicity might affect not only the lungs, as the portal of entry, but also other organs and tissues, for example, the liver, where the nanofibers could be translocated. Therefore, further long-term studies are required to elucidate the effects and modes of action of different types of CNF. These studies should be combined with exposure measurements that could allow us to perform an appropriate assessment of the associated risks.

ASSOCIATED CONTENT

Supporting Information

The Supporting Information is available free of charge at https://pubs.acs.org/doi/10.1021/acs.biomac.2c00072.

Field-emission scanning electron microscopy images of CNFs; body weight gain in mice exposed to CNF samples; bronchoalveolar lavage fluid cellularity after CNF exposure; histological analyses of lung samples at 1-, 28-, and 90-days post-exposure to CNFs; and frequency of micronucleated peripheral blood erythrocytes after CNF exposure (PDF)

AUTHOR INFORMATION

Corresponding Author

Julia Catalán − *Finnish Institute of Occupational Health, 00032 Helsinki, Finland; Department of Anatomy, Embryology and Genetics, University of Zaragoza, 50013 Zaragoza, Spain;* orcid.org/0000-0003-2936-242X; Email: julia.catalan@ttl.fi

Authors

Kukka Aimonen − *Finnish Institute of Occupational Health, 00032 Helsinki, Finland*

Mira Hartikainen − *Finnish Institute of Occupational Health, 00032 Helsinki, Finland*

Monireh Imani − *Department of Bioproducts and Biosystems, Aalto University, 02150 Espoo, Finland;* orcid.org/0000-0002-0893-8429

Satu Suhonen − *Finnish Institute of Occupational Health, 00032 Helsinki, Finland*

Gerard Vales − *Finnish Institute of Occupational Health, 00032 Helsinki, Finland*

Carlos Moreno − *Department of Anatomy, Embryology and Genetics, University of Zaragoza, 50013 Zaragoza, Spain*

Hanna Saarelainen − *Finnish Institute of Occupational Health, 00032 Helsinki, Finland*

Kirsi Siivola − *Finnish Institute of Occupational Health, 00032 Helsinki, Finland*

Esa Vanhala − *Finnish Institute of Occupational Health, 00032 Helsinki, Finland*

Henrik Wolff − *Finnish Institute of Occupational Health, 00032 Helsinki, Finland*

Orlando J. Rojas − *Department of Bioproducts and Biosystems, Aalto University, 02150 Espoo, Finland; Bioproducts Institute, Department of Chemical and Biological Engineering, Department of Chemistry and Department of Wood Science, The University of British Columbia, Vancouver BC V6T 1Z3, Canada;* orcid.org/0000-0003-4036-4020

Hannu Norppa − *Finnish Institute of Occupational Health, 00032 Helsinki, Finland*

Complete contact information is available at: https://pubs.acs.org/10.1021/acs.biomac.2c00072

Author Contributions

The article was written through contributions of all authors. All authors have given approval to the final version of the article.

Funding

The work in this article was supported by the Finnish Work Environment Fund (project no. 117146). O.J.R. and M.I. acknowledge additional funding support from the European Research Council under the European Union's Horizon 2020 research and innovation program (ERC Advanced grant agreement no. 788489, "BioElCell").

Notes

The authors declare no competing financial interest.

■ ACKNOWLEDGMENTS

The authors would like to thank UPM Kymmene Oy for supplying the bleached sulfite birch-dissolving pulp. The animal facilities and the processing of tissue samples for TEM analyses were outsourced to the Laboratory Animal Center and the Electron Microscopy Core Unit, respectively, of the University of Helsinki. The authors also wish to thank Sauli Savukoski for his excellent technical assistance.

■ REFERENCES

(1) Li, T.; Chen, C.; Brozena, A. H.; Zhu, J. Y.; Xu, L.; Driemeier, C.; Dai, J.; Rojas, O. J.; Isogai, A.; Wågberg, L.; Hu, L. Developing fibrillated cellulose as a sustainable technological material. *Nature* **2021**, *590*, 47−56.

(2) Ogura, I.; Kotake, M.; Kuboyama, T.; Kajihara, H. Measurements of cellulose nanofiber emissions and potential exposures at a production facility. *NanoImpact* **2020**, *20*, 100273.

(3) Lopes, V. R.; Sanchez-Martinez, C.; Strømme, M.; Ferraz, N. In vitro biological responses to nanofibrillated cellulose by human dermal, lung and immune cells: surface chemistry aspect. *Part. Fiber Toxicol.Fiber* **2017**, *14*, 1.

(4) Foster, E. J.; Moon, R. J.; Agarwal, U. P.; Bortner, M. J.; Bras, J.; Camarero-Espinosa, S.; Chan, K. J.; Clift, M. J. D.; Cranston, E. D.; Eichhorn, S. J.; Fox, D. M.; Hamad, W. Y.; Heux, L.; Jean, B.; Korey, M.; Nieh, W.; Ong, K. J.; Reid, M. S.; Renneckar, S.; Roberts, R.; Shatkin, J. A.; Simonsen, J.; Stinson-Bagby, K.; Wanasekara, N.; Youngblood, J. Current characterization methods for cellulose nanomaterials. *Chem. Soc. Rev.* **2018**, *47*, 2609−2679.

(5) Chinga-Carrasco, G.; Rosendahl, J.; Catalán, J. Nanocellulose - Nanotoxicology, safety aspects and 3D printing. *Adv. Exp. Med. Biol.* **2021**, *1357*, 155−177.

(6) Berto, G. L.; Mattos, B. D.; Rojas, O. J.; Arantes, V. Single-Step Fiber Pretreatment with Monocomponent Endoglucanase: Defibrillation Energy and Cellulose Nanofibril Quality. *ACS Sustainable Chem. Eng.* **2021**, *9*, 2260−2270.

(7) Lavoine, N.; Desloges, I.; Dufresne, A.; Bras, J. Microfibrillated cellulose − Its barrier properties and applications in cellulosic materials: A review. *Carbohydr. Polym.* **2012**, *90*, 735−764.

(8) Rol, F.; Belgacem, M. N.; Gandini, A.; Bras, J. Recent advances in surface-modified cellulose nanofibrils. *Prog. Polym. Sci.* **2019**, *88*, 241−264.

(9) Desmaisons, J.; Boutonnet, E.; Rueff, M.; Dufresne, A.; Bras, J. A new quality index for benchmarking of different cellulose nanofibrils. *Carbohydr. Polym.* **2017**, *174*, 318−329.

(10) Saito, T.; Hirota, M.; Tamura, N.; Kimura, S.; Fukuzumi, H.; Heux, L.; Isogai, A. Individualization of Nano-Sized Plant Cellulose Fibrils by Direct Surface Carboxylation Using TEMPO Catalyst under Neutral Conditions. *Biomacromolecules* **2009**, *10*, 1992−1996.

(11) Catalán, J.; Norppa, H. Safety Aspects of Bio-Based Nanomaterials. *Bioengineering* **2017**, *4*, 94.

(12) Ede, J.; Ong, K.; Goergen, M.; Rudie, A.; Pomeroy-Carter, C.; Shatkin, J. Risk Analysis of Cellulose Nanomaterials by Inhalation: Current State of Science. *Nanomaterials* **2019**, *9*, 337.

(13) Stefaniak, A. B.; Seehra, M. S.; Fix, N. R.; Leonard, S. S. Lung biodurability and free radical production of cellulose nanomaterials. *Inhal. Toxicol.* **2014**, *26*, 733−749.

(14) Lindberg, H. K.; Catalán, J.; Aimonen, K. J.; Wolff, H.; Wedin, I.; Nuopponen, M.; Savolainen, K. M.; Norppa, H. Evaluation of the genotoxic potential of different types of nanofibrillated celluloses. *TechConnect Briefs* **2017**, *1*, 229−232.

(15) Ilves, M.; Vilske, S.; Aimonen, K.; Lindberg, H. K.; Pesonen, S.; Wedin, I.; Nuopponen, M.; Vanhala, E.; Højgaard, C.; Winther, J. R.; Willemoës, M.; Vogel, U.; Wolff, H.; Norppa, H.; Savolainen, K.; Alenius, H. Nanofibrillated cellulose causes acute pulmonary inflammation that subsides within a month. *Nanotoxicology* **2018**, *12*, 729−746.

(16) Shanmugam, K.; Doosthosseini, H.; Varanasi, S.; Garnier, G.; Batchelor, W. Nanocellulose films as air and water vapour barriers: A recyclable and biodegradable alternative to polyolefin packaging. *Sustainable Mater. Technol.* **2019**, *22*, No. e00115.

(17) Ventura, C.; Pinto, F.; Lourenço, A. F.; Ferreira, P. J. T.; Louro, H.; Silva, M. J. On the toxicity of cellulose nanocrystals and nanofibrils in animal and cellular models. *Cellulose* **2020**, *27*, 5509−5544.

(18) Lopes, V. R.; Strømme, M.; Ferraz, N. In vitro biological impact of nanocellulose fibers on human gut bacteria and gastrointestinal cells. *Nanomaterials* **2020**, *10*, 1159.

(19) Aimonen, K.; Suhonen, S.; Hartikainen, M.; Lopes, V. R.; Norppa, H.; Ferraz, N.; Catalán, J. Role of Surface Chemistry in the In Vitro Lung Response to Nanofibrillated Cellulose. *Nanomaterials* **2021**, *11*, 389.

(20) Catalán, J.; Rydman, E.; Aimonen, K.; Hannukainen, K. S.; Suhonen, S.; Vanhala, E.; Moreno, C.; Meyer, V.; Perez, D. D.; Sneck, A.; Forsström, U.; Højgaard, C.; Willemoes, M.; Winther, J. R.; Vogel, U.; Wolff, H.; Alenius, H.; Savolainen, K. M.; Norppa, H. Genotoxic and inflammatory effects of nanofibrillated cellulose in murine lungs. *Mutagenesis* **2017**, *32*, 23−31.

(21) Park, E.-J.; Khaliullin, T. O.; Shurin, M. R.; Kisin, E. R.; Yanamala, N.; Fadeel, B.; Chang, J.; Shvedova, A. A. Fibrous nanocellulose, crystalline nanocellulose, carbon nanotubes, and crocidolite asbestos elicit disparate immune responses upon pharyngeal aspiration in mice. *J. Immunot.* **2018**, *15*, 12−23.

(22) Hadrup, N.; Knudsen, K. B.; Berthing, T.; Wolff, H.; Bengtson, S.; Kofoed, C.; Espersen, R.; Højgaard, C.; Winther, J. R.; Willemoës, M.; Wedin, I.; Nuopponen, M.; Alenius, H.; Norppa, H.; Wallin, H.; Vogel, U. Pulmonary effects of nanofibrillated celluloses in mice suggest that carboxylation lowers the inflammatory and acute phase responses. *Environ. Toxicol. Pharmacol.* **2019**, *66*, 116−125.

(23) Shvedova, A. A.; Kisin, E.; Murray, A. R.; Johnson, V. J.; Gorelik, O.; Arepalli, S.; Hubbs, A. F.; Mercer, R. R.; Keohavong, P.; Sussman, N.; Jin, J.; Yin, J.; Stone, S.; Chen, B. T.; Deye, G.; Maynard, A.; Castranova, V.; Baron, P. A.; Kagan, V. E. Inhalation vs. aspiration of single-walled carbon nanotubes in C57BL/6 mice: inflammation, fibrosis, oxidative stress, and mutagenesis. *Am. J. Physiol. Lung Cell Mol. Physiol.* **2008**, *295*, L552−L565.

(24) Liu, J.; Bacher, M.; Rosenau, T.; Willför, S.; Mihranyan, A. Potentially Immunogenic Contaminants in Wood-Based and Bacterial Nanocellulose: Assessment of Endotoxin and (1,3)-β-d-Glucan Levels. *Biomacromolecules* **2018**, *19*, 150−157.

(25) Li, Y.; Boraschi, D. Endotoxin contamination: a key element in the interpretation of nanosafety studies. *Nanomedicine* **2016**, *11*, 269−287.

(26) Giannakou, C.; Aimonen, K.; Bloois, L. V.; Catalán, J.; Geertsma, R. E.; Gremmer, E. R.; de Jong, W. H.; Keizers, P. H.; Schwillens, P. L.; Vandebriel, R. J.; Park, M. V. Sensitive method for endotoxin determination in nanomedicinal product samples. *Nanomedicine* **2019**, *14*, 1231−1246.

(27) Aimonen, K.; Imani, M.; Hartikainen, M.; Suhonen, S.; Vanhala, E.; Moreno, C.; Rojas, O. J.; Norppa, H.; Catalán, J. Surface functionalization and size modulate the formation of reactive oxygen species and genotoxic effects of cellulose nanofibrils. *Part. Fiber Toxicol.Fiber* **2022**, *19*, 19.

https://doi.org/10.1021/acs.biomac.2c00072
Biomacromolecules 2022, 23, 2752−2766

(28) Sai, T.; Maru, J.; Obara, S.; Endoh, S.; Kajihara, H.; Fujita, K. Screening of preservatives and evaluation of sterilized cellulose nanofibers for toxicity studies. *J. Occup. Health* **2020**, *62*, No. e12176.
(29) Imani, M.; Dimic-Misic, K.; Tavakoli, M.; Rojas, O. J.; Gane, P. A. C. Coupled Effects of Fibril Width, Residual and Mechanically Liberated Lignin on the Flow, Viscoelasticity, and Dewatering of Cellulosic Nanomaterials. *Biomacromolecules* **2020**, *21*, 4123−4134.
(30) Imani, M.; Ghasemian, A.; Dehghani-Firouzabadi, M. R.; Afra, E.; Borghei, M.; Johansson, L. S.; Gane, P. A. C.; Rojas, O. J. Coupling Nanofibril Lateral Size and Residual Lignin to Tailor the Properties of Lignocellulose Films. *Adv. Mater. Interfaces* **2019**, *6*, 1900770.
(31) Im, W.; Lee, S.; Rajabi Abhari, A.; Youn, H. J.; Lee, H. L. Optimization of carboxymethylation reaction as a pretreatment for production of cellulose nanofibrils. *Cellulose* **2018**, *25*, 3873−3883.
(32) Ventura, C.; Lourenço, A.; Ferreira, P. J. T.; Silva, M. J. Evaluating the genotoxicity of cellulose nanofibrils in a co-culture of human lung epithelial cells and monocyte-derived macrophages. *Toxicol. Lett.* **2018**, *291*, 173−183.
(33) Sanchez-Salvador, J. L.; Campano, C.; Negro, C.; Monte, M. C.; Blanco, A. Increasing the Possibilities of TEMPO-Mediated Oxidation in the Production of Cellulose Nanofibers by Reducing the Reaction Time and Reusing the Reaction Medium. *Adv. Sustainable Syst.* **2021**, *5*, 2000277.
(34) Saito, T.; Isogai, A. Introduction of aldehyde groups on surfaces of native cellulose fibers by TEMPO-mediated oxidation. *Colloids Surf., A* **2006**, *289*, 219−225.
(35) Bitounis, D.; Pyrgiotakis, G.; Bousfield, D.; Demokritou, P. Dispersion preparation, characterization, and dosimetric analysis of cellulose nano-fibrils and nano-crystals: Implications for cellular toxicological studies. *NanoImpact* **2019**, *15*, 100171.
(36) Porter, D. W.; Hubbs, A. F.; Mercer, R. R.; Wu, N.; Wolfarth, M. G.; Sriram, K.; Leonard, S.; Battelli, L.; Schwegler-Berry, D.; Friend, S.; Andrew, M.; Chen, B. T.; Tsuruoka, S.; Endo, M.; Castranova, V. Mouse pulmonary dose- and time course-responses induced by exposure to multi-walled carbon nanotubes. *Toxicology* **2010**, *269*, 136−147.
(37) Yanamala, N.; Farcas, M. K.; Kisin, E. R.; Kagan, V. E.; Geraci, C. L.; Shvedova, A. A. In vivo evaluation of the pulmonary toxicity of cellulose nanocrystals: A renewable and sustainable nanomaterial of the future. *ACS Sustainable Chem. Eng.* **2014**, *2*, 1691−1698.
(38) Shvedova, A. A.; Kisin, N.; Farcas, M. T.; Menas, A. L.; Williams, A.; Fournier, P. M.; Reynolds, J. S.; Gutkin, D. W.; Star, A.; Reiner, R. S.; Halappanavar, S.; Kagan, V. E. Gender differences in murine pulmonary responses elicited by cellulose nanocrystals. *Part. Fiber Toxicol.Fiber* **2016**, *13*, 28.
(39) Catalán, J.; Siivola, K. M.; Nymark, P.; Lindberg, H.; Suhonen, S.; Järventaus, H.; Koivisto, A. J.; Moreno, C.; Vanhala, E.; Wolff, H.; Kling, K. I.; Jensen, K. A.; Savolainen, K.; Norppa, H. In vitro and in vivo genotoxic effects of straight versus tangled multi-walled carbon nanotubes. *Nanotoxicology* **2016**, *10*, 794−806.
(40) OECD. *Test No. 474: Mammalian Erythrocyte Micronucleus Test*, 2016. https://doi.org/10.1787/9789264264762-en (accessed on 13 Jan 2022).
(41) Nordli, H. R.; Chinga-Carrasco, A. M.; Pukstad, B. Producing ultrapure wood cellulose nanofibrils and evaluating the cytotoxicity using human skin cells. *Carbohydr. Polym.* **2016**, *150*, 65−73.
(42) Johnston, C. J.; Finkelstein, J. N.; Gelein, R.; Oberdörster, G. Pulmonary cytokine and chemokine mRNA levels after inhalation of lipopolysaccharide in C57BL/6 mice. *Toxicol. Sci.* **1998**, *46*, 300−307.
(43) Poulsen, S. S.; Jackson, P.; Kling, K.; Knudsen, K. B.; Skaug, V.; Kyjovska, Z. O.; Thomsen, B. L.; Clausen, P. A.; Atluri, R.; Berthing, T.; Bengtson, S.; Wolff, H.; Jensen, K. A.; Wallin, H.; Vogel, U. Multi-walled carbon nanotube physicochemical properties predict pulmonary inflammation and genotoxicity. *Nanotoxicology* **2016**, *10*, 1263−1275.
(44) Rydman, E. M.; Ilves, M.; Vanhala, E.; Vippola, M.; Lehto, M.; Kinaret, P. A. S.; Pylkkänen, L.; Happo, M.; Hirvonen, M.-R.; Greco, D.; Savolainen, K.; Wolff, H.; Alenius, H. A Single Aspiration of Rod-like Carbon Nanotubes Induces Asbestos-like Pulmonary Inflammation Mediated in Part by the IL-1 Receptor. *Toxicol. Sci.* **2015**, *147*, 140−155.
(45) Lindberg, H. K.; Falck, G. C.-M.; Suhonen, S.; Vippola, M.; Vanhala, E.; Catalán, J.; Savolainen, K.; Norppa, H. Genotoxicity of nanomaterials: DNA damage and micronuclei induced by carbon nanotubes and graphite nanofibers in human bronchial epithelial cells in vitro. *Toxicol. Lett.* **2009**, *186*, 166−173.
(46) Hadrup, N.; Rahmani, F.; Jacobsen, N. R.; Saber, A. T.; Jackson, P.; Bengtson, S.; Williams, A.; Wallin, H.; Halappanavar, S.; Vogel, U. Acute phase response and inflammation following pulmonary exposure to low doses of zinc oxide nanoparticles in mice. *Nanotoxicology* **2019**, *13*, 1275−1292.
(47) Bright, J.; Aylott, M.; Bate, S.; Geys, H.; Jarvis, P.; Saul, J.; Vonk, R. Recommendations on the statistical analysis of the Comet assay. *Pharm. Stat.* **2011**, *10*, 485−493.
(48) FDA—US Food and Drug Administration. Bacterial Endotoxins/Pyrogens, 2014. https://www.fda.gov/inspections-compliance-enforcement-and-criminal-investigations/inspection-technical-guides/bacterial-endotoxinspyrogens (accessed 13 Jan, 2022).
(49) Chen, Y.; Geng, B.; Ru, J.; Tong, C.; Liu, H.; Chen, J. Comparative characteristics of TEMPO-oxidized cellulose nanofibers and resulting nanopapers from bamboo, softwood, and hardwood pulps. *Cellulose* **2017**, *24*, 4831−4844.
(50) Donaldson, K.; Murphy, F. A.; Duffin, R.; Poland, C. A. Asbestos, carbon nanotubes and the pleural mesothelium: a review of the hypothesis regarding the role of long fiber retention in the parietal pleura, inflammation and mesothelioma. *Part. Fiber Toxicol.Fiber* **2010**, *7*, 5.
(51) Nagai, H.; Okazaki, Y.; Chew, S. H.; Misawa, N.; Yamashita, Y.; Akatsuka, S.; Ishihara, T.; Yamashita, K.; Yoshikawa, Y.; Yasui, H.; Jiang, L.; Ohara, H.; Takahashi, T.; Ichihara, G.; Kostarelos, K.; Miyata, Y.; Shinohara, H.; Toyokuni, S. Diameter and rigidity of multiwalled carbon nanotubes are critical factors in mesothelial injury and carcinogenesis. *Proc. Natl. Acad. Sci.* **2011**, *108*, E1330−E1338.
(52) Donaldson, K.; Poland, C. A. Inhaled nanoparticles and lung cancer - what we can learn from conventional particle toxicology. *Swiss Med. Wkly.* **2012**, *142*, w13547.
(53) Cullen, R. T.; Searl, A.; Miller, B. G.; Davis, J. M. G.; Jones, A. D. Pulmonary and intraperitoneal inflammation induced by cellulose fibers. *J. Appl. Toxicol.* **2000**, *20*, 49−60.
(54) Køibler, C.; Poulsen, S. S.; Saber, A. T.; Jacobsen, N. R.; Wallin, H.; Yauk, C. L.; Halappanavar, S.; Vogel, U.; Qvortrup, K.; Mølhave, K. Time-dependent subcellular distribution and effects of carbon nanotubes in lungs of mice. *PLoS One* **2015**, *10*, No. e0116481.
(55) Sabo-Attwood, T.; Ramos-Nino, M.; Bond, J.; Butnor, K. J.; Heintz, N.; Gruber, A. D.; Steele, C.; Taatjes, D. J.; Vacek, P.; Mossman, B. T. Gene Expression Profiles Reveal Increased mClca3 (Gob5) Expression and Mucin Production in a Murine Model of Asbestos-Induced Fibrogenesis. *Am. J. Pathol.* **2005**, *167*, 1243−1256.
(56) Evans, S. J.; Clift, M. J. D.; Singh, N.; Wills, J. W.; Hondow, N.; Wilkinson, T. S.; Burgum, M. J.; Brown, A. P.; Jenkins, G. J.; Doak, S. H. In vitro detection of in vitro secondary mechanisms of genotoxicity induced by engineered nanomaterials. *Part. Fiber Toxicol.Fiber* **2019**, *16*, 8.
(57) Li, J.; Wang, X.; Chang, C. H.; Jiang, J.; Liu, Q.; Liu, X.; Liao, Y. P.; Ma, T.; Meng, H.; Xia, T. Nanocellulose Length Determines the Differential Cytotoxic Effects and Inflammatory Responses in Macrophages and Hepatocytes. *Small* **2021**, *17*, No. e2102545.
(58) Murray, R. A.; Escobar, A.; Bastús, N. G.; Andreozzi, P.; Puntes, V.; Moya, S. E. Fluorescently labelled nanomaterials in nanosafety research: Practical advice to avoid artefacts and trace unbound dye. *NanoImpact* **2018**, *9*, 102−113.
(59) Knudsen, K. B.; Berthing, T.; Jackson, P.; Poulsen, S. S.; Mortensen, A.; Jacobsen, N. R.; Skaug, V.; Szarek, J.; Hougaard, K. S.; Wolff, H.; Wallin, H.; Vogel, U. Physicochemical predictors of Multi-Walled Carbon Nanotube-induced pulmonary histopathology and toxicity one year after pulmonary deposition of 11 different Multi-Walled Carbon Nanotubes in mice. *Basic Clin. Pharmacol. Toxicol.* **2019**, *124*, 211−227.

https://doi.org/10.1021/acs.biomac.2c00072
Biomacromolecules 2022, 23, 2752−2766

(60) Modrzynska, J.; Berthing, T.; Ravn-Haren, G.; Jacobsen, N. R.; Weydahl, I. K.; Loeschner, K.; Mortensen, A.; Saber, A. T.; Vogel, U. Primary genotoxicity in the liver following pulmonary exposure to carbon black nanoparticles in mice. *Part. Fiber Toxicol.Fiber* **2018**, *15*, 2.
(61) Gonzalez, L.; Kirsch-Volders, M. Biomonitoring of genotoxic effects for human exposure to nanomaterials: The challenge ahead. *Mutat. Res. Rev. Mutat. Res.* **2016**, *768*, 14−26.
(62) Kohl, Y.; Rundén-Pran, E.; Mariussen, E.; Hesler, M.; El Yamani, N.; Longhin, E. M.; Dusinska, M. Genotoxicity of Nanomaterials: Advanced In Vitro Models and High Throughput Methods for Human Hazard Assessment—A Review. *Nanomaterials* **2020**, *10*, 1911.
(63) Sadauskas, E.; Jacobsen, N. R.; Danscher, G.; Stoltenberg, M.; Vogel, U.; Larsen, A.; Kreyling, W.; Wallin, H. Biodistribution of gold nanoparticles in mouse lung following intratracheal instillation. *Chem. Cent. J.* **2009**, *3*, 16.
(64) Wheeler, M. D. Endotoxin and Kupffer cell activation in alcoholic liver disease. *Alcohol Res. Health* **2003**, *27*, 300−306.

https://doi.org/10.1021/acs.biomac.2c00072
Biomacromolecules 2022, 23, 2752−2766